


Synovium-Derived Mesenchymal Stem Cell-Based Scaffold-Free Fibrocartilage Engineering for Bone–Tendon Interface Healing in an Anterior Cruciate Ligament Reconstruction Model

Sujin Noh¹ · Sang Jin Lee² · James J. Yoo² · Yong Jun Jin³ · Hee-Woong Yun⁴ ·
Byoung-Hyun Min² · Jae-Young Park⁶ · Do Young Park^{1,2,3,4,5} 

Received: 23 June 2023 / Revised: 21 August 2023 / Accepted: 27 August 2023 / Published online: 19 October 2023
© Korean Tissue Engineering and Regenerative Medicine Society 2023

Abstract

BACKGROUND: Current tendon and ligament reconstruction surgeries rely on scar tissue healing which differs from native bone-to-tendon interface (BTI) tissue. We aimed to engineer Synovium-derived mesenchymal stem cells (Sy-MSCs) based scaffold-free fibrocartilage constructs and investigate *in vivo* bone–tendon interface (BTI) healing efficacy in a rat anterior cruciate ligament (ACL) reconstruction model.

METHODS: Sy-MSCs were isolated from knee joint of rats. Scaffold-free sy-MSC constructs were fabricated and cultured in differentiation media including TGF- β -only, CTGF-only, and TGF- β + CTGF. Collagenase treatment on tendon grafts was optimized to improve cell-to-graft integration. The effects of fibrocartilage differentiation and collagenase treatment on BTI integration was assessed by conducting histological staining, cell adhesion assay, and tensile testing. Finally, histological and biomechanical analyses were used to evaluate *in vivo* efficacy of fibrocartilage construct in a rat ACL reconstruction model.

RESULTS: Fibrocartilage-like features were observed with in the scaffold-free sy-MSC constructs when applying TGF- β and CTGF concurrently. Fifteen minutes collagenase treatment increased cellular attachment 1.9-fold compared to the Control group without affecting tensile strength. The failure stress was highest in the Col + D + group (22.494 ± 13.74 Kpa) compared to other groups at integration analysis *in vitro*. The ACL Recon + FC group exhibited a significant 88% increase in estimated stiffness ($p = 0.0102$) compared to the ACL Recon group at the 4-week postoperative period.

CONCLUSION: Scaffold-free, fibrocartilage engineering together with tendon collagenase treatment enhanced fibrocartilaginous BTI healing in ACL reconstruction.

Keywords Anterior cruciate ligament reconstruction · Tendon graft remodeling · Scaffold-free tissue engineering

Sujin Noh and Sang Jin Lee are contributed equally to this work.

✉ Do Young Park
theboy@ajou.ac.kr

¹ Department of Biomedical Sciences, Graduate School of Ajou University, 206 World Cup-Ro, Yeongtong-Gu, Suwon, Republic of Korea

² Wake Forest Institute for Regenerative Medicine, Wake Forest School of Medicine, Winston-Salem, NC 27157, USA

³ Department of Orthopedic Surgery, School of Medicine, Ajou University, Suwon, Republic of Korea

⁴ Cell Therapy Center, Ajou Medical Center, Suwon, Republic of Korea

⁵ Leading Convergence of Healthcare and Medicine, Institute of Science & Technology (ALChEMIST), Ajou University, Suwon, Republic of Korea

⁶ Department of Orthopedics Surgery, CHA University Bundang Medical Center, Bundang-Gu, Seongnam-Si, Gyeonggi-Do, Republic of Korea

1 Introduction

Bone–tendon interface (BTI) injuries are one of the most commonly injured anatomical structures in the orthopedic field, with more than 30 million injuries occurring worldwide [1]. Most commonly affected areas include the anterior cruciate ligament (ACL) in the knee and rotator cuff of the shoulder, with 48% of ACL injuries occurring in the BTI area [2]. Due to its transitional composition of tissue and high biomechanical loads, BTI injuries often require surgical intervention. The annual incidence of ACL injuries is 30–78 per 100,000 persons [3, 4], requiring 400,000 ACL reconstructions annually worldwide [6]. While ACL reconstruction result in functional improvement and return to sports, graft retears and residual instability occur in 8–25% of patients [7] leading to revision surgeries in 17.5% of patients [8]. This is, in part, due to the defective healing in the BTI [9].

During ligament reconstructions, the tendon graft is fixed in a bone tunnel. BTI healing occurs via scar tissue formation between the tendon graft and bone. Scar tissue, which is disorganized and biomechanically inferior compared to fibrocartilage, may lead to a high failure rate and unsatisfactory clinical outcomes [10, 11]. This occurrence is caused by the lack of a gradient mineral distribution and collagen fiber disruption, which are essential to the native BTI's microstructure and metabolic activity [12]. A variety of bioinspired materials and related fabrication techniques including 3D printing [13, 14] and electrospinning [16, 17] were utilized to mimic the inherent hierarchical structures of BTI, with showing the usefulness of multiphasic scaffolds for reconstruction of the BTI [18, 19]. Nevertheless, the biggest obstacle to functional BTI healing is still obtaining a progressive change in physiological characteristics [20]. To address this issue, previous studies aimed to improve the BTI healing process via osteoinductive materials [21, 22] and stem cells [23–30]. Cell therapies targeting BTI utilizing bone marrow-derived mesenchymal stem cells (BM-MSCs), Synovium-derived mesenchymal stem cells (Sy-MSCs), and periosteal progenitor cells have been reported, resulting in some biomechanical and histologic benefits. To improve delivery of cells, Lui et al. utilized tendon-derived stem cell sheets rather than individual cells to wrap the transplanted graft, which resulted in improved healing without the use of scaffolds [32]. In terms of biomimicry, however, there is an unmet clinical need to repair BTI via fibrocartilage with a level of integration comparable to that observed in the native tissue.

The BTI, also known as the enthesis, is a highly specialized transitional tissue consisting of tendon, non-mineralized, mineralized fibrocartilage, and bone. These structural characteristics lead to gradual mechanical

property changes allowing progressive transmission of mechanical loads from tendon to bone and withstanding load from various vectors [33]. We have previously developed scaffold-free cartilage constructs that resulted in not only excellent biomimicry toward cartilage, but also improved cell delivery and preservation of the transplanted construct after 6 months in a non-human primate model [34]. We aimed to engineer sy-MSC based scaffold-free fibrocartilage constructs and investigate *in vivo* BTI healing efficacy in a rat ACL reconstruction model. We hypothesized that the use of scaffold-free, fibrocartilage neo-tissue would promote fibrocartilage-like tissue healing in the BTI.

2 Materials and methods

2.1 Cell isolation and culture

All animal procedures were performed according to the protocol (A16-141) approved by the Institutional Animal Care and Use Committee (IACUC) at Wake Forest University Health Sciences. Three male Sprague-Dawley rats were used. The synovium of knee joints from the rats were harvested from the anterior fat pad. Tissues were minced, treated for 4 h at 37 °C with 0.2% type II collagenase (Worthington Biochemical Corp., Freehold, NJ, USA), and centrifuged at 1500 rpm for 10 min. After washing twice with complete growth medium (CGM; α -MEM containing 10% FBS, 100 U/ml penicillin G, and 100 μ g/ml streptomycin), the digested tissue was passed through 100 μ m nylon mesh filter (Falcon, BD Bioscience, Franklin Lakes, NJ, USA) to yield single-cell suspensions. Rat synovium-derived mesenchymal stem cells (rSy-MSCs) were counted with a hemocytometer and seeded at a density of 8×10^3 cells/cm². After 3 days, the medium was changed to remove non-adherent cells and incubated at 37°C with 5% CO₂. rSy-MSCs were passaged at 70–80% confluence and cells at passages under 4 were used in this study.

2.2 Scaffold-free fibrocartilage construct fabrication

Schematic figure of experimental flow was suggested as Fig. 1. The effects of transforming growth factor beta-3 (TGF- β) and connective tissue growth factor (CTGF) on fibrocartilage construct fabrication were compared. 4×10^6 of rSy-MSCs were seeded at 60 mm tissue culture dish. After 24 h following cell seeding, cells were scraped with a cell lifter (Corning, New York, US) and placed 6 well plate with cell growth media. Subsequently, the medium was changed to differentiation medium (DM; high glucose

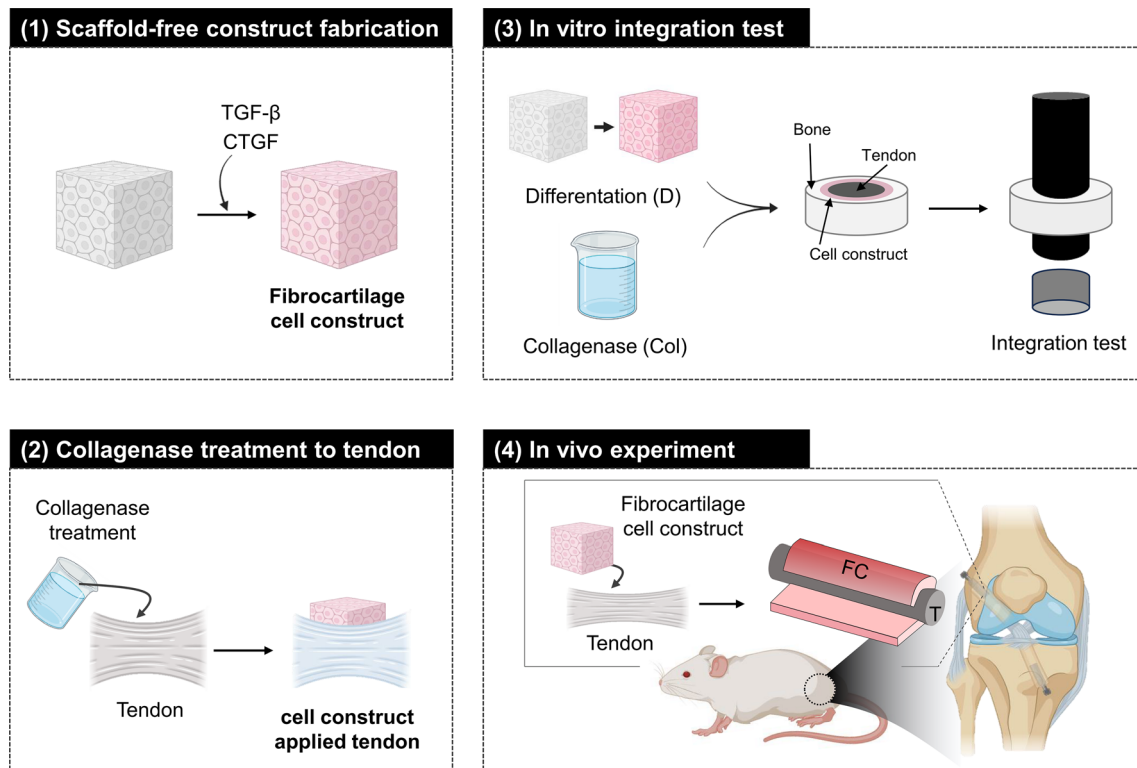


Fig. 1 Schematic overview of scaffold-free fibrocartilage engineering for bone-tendon interface healing

DMEM supplemented with 1% insulin, transferrin, sodium selenite (ITS) + mix, 50 $\mu\text{g}/\text{mL}$ ascorbic acid-2-phosphate, 100 nM dexamethasone, 1% penicillin–streptomycin, 100 $\mu\text{g}/\text{mL}$ sodium pyruvate, and 40 $\mu\text{g}/\text{mL}$ L-proline) with two growth factors (10 ng/mL of TGF- β and 100 ng/mL of CTGF all from Sigma-Aldrich, St. Louis, MO, USA) or without (control group) two growth factors. Subsequently, the constructs were cultured in DM for 2 weeks to induce differentiation in the respective growth factor groups.

For sulfated glycosaminoglycans (sGAG) content analysis, freeze-dried samples were weighed and digested in papain solution with 125 mg/mL papain with 5 mM L-cysteine, 100 mM Na_2HPO_4 , 5 mM EDTA (Sigma-Aldrich) at 60 $^\circ\text{C}$ for 16 h as previously reported [34]. The amount of sGAG was quantified with Blyscan Assay following the manufacturer's instructions (B1000, Biocolor, Carrickfergus, UK).

For collagen content analysis, freeze-dried samples were solubilized in 0.1M HCl with 0.1% (w/v) pepsin at RT for 24 h. The amount of collagen was quantified with Sircol Collagen Assay (SCA) following the manufacturer's instructions (S1000, Biocolor).

For histological analysis, samples were fixed with 10% formalin for 24 h at room temperature (RT) and then embedded in paraffin wax. Sample slides in 5 μm thickness were made and stained with safranin-O (Sigma-Aldrich) to examine the degree of GAG deposition. Other slides were

used to immunostain collagen type I (1:100, Abcam) and collagen type II (1:100, Abcam) antibodies using an immunohistochemical assay kit (GBI labs, Bothell, WA, USA).

For gene expression analysis, fibrocartilage constructs were homogenized with Biomasher (OPTIMA INC, Tokyo, Japan) on day 14. Total RNA was extracted from cells using Trizol reagent (Invitrogen Carlsbad, CA, USA) according to the manufacturer's instructions. Total RNA (500 ng) in a 20 μl mixed solution was reverse-transcribed into cDNA by iScript cDNA synthesis kit (Bio-Rad, Hercules, CA, USA). RT-qPCR was performed in a CFX96 Touch Real-time PCR Detection System (Bio-Rad) using SYBR Green detection (Roche, Mannheim, Germany). The mRNA expression levels of samples were normalized to GAPDH (glyceraldehyde-3-phosphate dehydrogenase) as a housekeeping gene and calculated by using the comparative CT method. Expression of genes including collagen type I (COL1A1), collagen type II (COL2A1), and aggrecan (ACAN) were analyzed. The primers used are shown in Supplemental Table 1.

2.3 Collagenase treatment on tendon

A sheath known as the paratenon may deter BTI integration and are usually dissected off during ACL autograft reconstructions [35]. In addition to this idea, collagenase

treatment was utilized to improve the attachment of rSy-MSCs on the surface of the flexor digitorum profundus (FDP) tendon graft. The volume of collagenase was optimized to induce slight digestion of the tendon surface which resulted in $0.5 \mu\text{l}/\text{mm}^2$. Briefly, a total of 18 (3 grafts for each group), $2 \text{ mm} \times 5 \text{ mm} \times 1 \text{ mm}$ FDP grafts were harvested from 9 rats. The effects of collagenase treatment were evaluated according to treatment time; 0, 5, 15, 30, 60 min. The group without any treatment was named as the control group. A mechanical abrasion group was also analyzed, where we applied mechanical abrasion by rubbing the tendon with sandpaper (220 grit) three times to the tendon surface for comparison with collagenase treatment. After treatment, the degree of integration with tendon and cells was evaluated by the histological observation and mechanical test.

Sirius red (SR) staining was used to clearly distinguish collagen fibers structure of tendon. Briefly, sample were incubated for 1 h in a 0.1% Sirius Red solution diluted in picric acid. After rinsing in 0.5% Glacial acetic acid, the samples were dehydrated and mounted using Permunt Mounting Medium (Fisher Scientific). All PSR imaging was performed on an axioscope 5 microscope (Zeiss) with linear polarizers (PSR-POL).

For cell adhesion analysis, 5×10^6 cells were labeled with PKH26 Red Fluorescent Cell Linker Mini Kit For General Cell Membrane Labeling (Sigma-Aldrich). Subsequently, cells were seeded on the tendon surface ($n = 3$). Following treatment, cells remaining on the cell culture plate that did not attach to the tendon surface were detached by from the culture plate using 0.05% trypsin (Gibco BRL) and counted with a hemocytometer. Finally, the percentage of cell adhesion was calculated by ratio of cell number counted from hemocytometer to initial seeding number of cells. Three independent experiments were repeated for the reliability.

Tensile test was performed by connecting the FDP with a length of 5 mm between two custom-made zigs. The pulling test was applied to measure the longitudinal axis strength, and this was carried out using a ZWICK/Roell Z005 testing machine with a 5 N loading cell (ZWICK/Roell, Ulm, Germany). The tests were performed with a 1 mm/min pulling rate for each sample. Loading values measured with a sensitivity of 0.1% by the device's load cell were entered into the software, and force values (F) were obtained; the tests were terminated after the detection of a force decrease and rupture of the sample. The Young's elastic modulus is typically calculated by analyzing the linear portion of the stress–strain curve, indicating the elastic resistance to compression.

2.4 *in vitro* bone/scaffold-free fibrocartilage construct/tendon integration

The effects of fibrocartilage differentiation and collagenase treatment were tested in an *in vitro* BTI reconstruction model. FDP tendons and bone tissue from the femur were obtained from pig carcasses (Finish pig, Yorkshire, female, >1 year, free of knee osteoarthritis) within 1 h of sacrifice. For bone preparation, cancellous bone was cut in to 6 mm diameter discs with 2 mm height. A cylinder-shaped defect (3 mm diameter) was created in the center using a 3 mm biopsy punch. For tendon tissue preparation, tendon samples were cut into 3 mm diameter, 2 mm height disc shapes perpendicular to the tendon fiber orientation. Overall, five groups were tested ($n = 6$ per group); (1) Empty (2) Col-D– (3) Col+D– (4) Col-D+ (5) Col+D+. Col+ groups were subjected to collagenase treatment of the tendon surface (15 min, 1% collagenase, $0.5 \mu\text{l}/\text{mm}^2$) before inserting the tendon disc into bone tissue. D+ groups were subjected to insertion of fibrocartilaginously differentiated scaffold-free construct using two growth factors, while D-groups were subjected to insertion of scaffold-free constructs cultured without growth factor treatment. After assembling the tendon tissues within the bone tissues, the *in vitro* BTI reconstruction constructs were cultured in high glucose DMEM supplemented with 1% ITS for 4 weeks. Afterwards, the histological and biomechanical evaluation was performed with these experimental groups.

For integration failure stress analysis, mechanical test using a push-out test was done as previously described [23]. While recording load, a specialized cylindrical-shaped indenter with 4-mm-diameter coupled with Universal testing machine pushed the inner tendon part with the rate of 1 mm/min. The load at failure and interface area were divided to compute failure stress (integration strength). TestXpert II was used for both the initial preparation of the tests and the post-test analysis of the data.

2.5 Bone-to-tendon healing *in vivo* efficacy

A total of 56 SD rats (27 weeks, 350g, Male) were used in this study. Rats were allocated in to 'ACL recon' group ($n = 28$), and 'ACL recon+FC' group ($n = 28$). Time points of 2 and 4 weeks were analyzed, with 14 animals allocated at each time point. The following is the brief description of the surgical procedure. The rats were anesthetized by 3% isoflurane with 2 L/min oxygen. Each rat was injected with dexmedetomidine (0.2 mg/Kg, IP) and ketamine (80 mg/Kg, IP). Oxygen (2 L/min) was delivered via a nose cone during the surgical procedure. Buprenorphine (0.1 mg/kg, SC) and meloxicam (1 mg/Kg, SC) were given after the induction. The left knee of the animals was shaved and

prepped in an aseptic manner. A lateral parapatellar incision was made. After patellar dislocation, the native ACL was removed. Bone tunnels were created with a 1mm diameter drill in the femur and tibia. FDP tendons were sutured at the ends and the suture was passed through the bone tunnels. The graft was seated at the native ACL site and fixed with 1.5 mm stainless steel cortical screws at the femur and tibia tunnel. For the ‘ACL recon+FC’ group, the FDP tendon graft was treated with collagenase as previously described at the proximal and distal ends of the tendon graft that come in contact with the bone tunnels. During graft passage, scaffold-free FC constructs were inserted in the bone tunnels in the surface opposite of the interference screws. Layer by layer closure of the skin was done. Postoperative analgesia was provided with meloxicam (0.1 mg/Kg, SC, qd for 4 days). The animals were single housed and fed ad libitum.

After euthanasia, 7 knees of each group and time point were analyzed for histology and biomechanical analysis, respectively. For biomechanical testing, the interferences screws were removed. All joint tissues were dissected off the knee joint excluding the ACL graft. The femur and tibial ends were placed on jigs in a biomechanical testing machine (ZWICK/Roell Z005, Ulm, Germany) directed along the longitudinal axis of the graft. After preloading of 1 N per specimen, ultimate failure load was calculated at a speed of 0.25 mm/s. Stiffness of constructs were calculated using TestXpert II.

2.6 Statistical analysis

Statistical analysis was conducted with Graph Pad Prism 8 (GraphPad Software, La Jolla, CA, USA) using one-way analysis of variance (ANOVA) with Tukey’s multiple comparison test as described in each assay. The data are expressed as means \pm SD. The statistical significance was determined as $*p < 0.05$, $**p < 0.01$, and $***p < 0.001$.

3 Results

3.1 Scaffold-free fibrocartilage construct fabrication *in vitro*

Safranin-O staining was strongly stained in the TGF- β group, but weakly stained in the control and CTGF group. CTGF+TGF- β group showed areas of strong safranin-O staining on the outer regions of the construct and weakly stained area in the center (Fig. 2A). Immunohistochemistry staining for collagen types I and II showed that the TGF- β group had more type II collagen, while the CTGF group had more type I collagen. CTGF+TGF- β group showed expression of both collagen types (Fig. 2A). Biochemical

quantification results showed the most sGAG expression in the TGF- β group, followed by CTGF+TGF- β group and CTGF group (Fig. 2B). Additionally, collagen contents were significantly higher in the CTGF group, but there was no significant difference between CTGF+TGF- β and other groups (Fig. 2B, Control: 9.987 ± 3.84 $\mu\text{g}/\text{mg}$, CTGF: 22.28 ± 6.97 $\mu\text{g}/\text{mg}$, CTGF+TGF- β : 16.99 ± 1.14 $\mu\text{g}/\text{mg}$, TGF- β : 19.68 ± 2.28 $\mu\text{g}/\text{mg}$). Moreover, the gene expression profile showed higher expression of COL1A1 with CTGF exposure, whereas chondrogenic marker, COL2A1 and ACAN expression were significantly increased upon TGF- β treatment (Fig. 2C). The CTGF + TGF- β group showed intermediate COL1A1, COL2A1 and ACAN expressions compared to CTGF and TGF- β treated groups. In all, histologic, biochemical and gene expression results showed elevated fibrocartilage features in the CTGF + TGF- β group.

3.2 Improvement of integration properties in tendon via collagenase treatment

Sirius red staining showed maintenance of collagen arrangement at tendon until 15 min collagenase treatment time (Fig. 3A). More than 30 min of collagenase treatment destroyed fibrillar crimp structure. At 60 min, dense fiber bundles were completely disorganized and collagen fluorescence decreased considerably. As shown Fig. 3A and B, cell attachment on tendon, on the other hand, increased according to collagenase treatment time (Control: $35.16 \pm 3.9\%$, Abrasion: $51.52 \pm 7.51\%$, 5 min: $56.46 \pm 5.57\%$, 15 min: $67.23 \pm 2.3\%$, 30 min: $75.08 \pm 2.77\%$, and 60 min: $80.85 \pm 2.1\%$). In collagenase treatment groups for >30 min, cells penetrated the tendon surface and adhered to the stroma (Fig. 3A). Tensile modulus was not considerably affected until collagenase treatment of 15 min, however, it reduced dramatically at >30 min (Fig. 3C, Control: 134.02 ± 38.57 Kpa, Abrasion: 124.7 ± 40.45 Kpa, 5 min: 120.93 ± 42.97 Kpa, 15 min: 120.93 ± 42.97 Kpa, 30 min: 75.58 ± 6.75 Kpa, and 60 min: 18.23 ± 8.65 Kpa). After these results, collagenase was applied to tendon for 15 min to improve cellular adhesion without altering tensile strength.

3.3 Integration analysis of scaffold-free fibrocartilage construct *in vitro*

Safranin-O stained tissue section revealed the presence of positive staining regardless of collagenase treatment in the group with fibrocartilage differentiation (Fig. 4A). Additionally, collagenase treatment to tendon showed enhanced integration of bone-to-scaffold-free fibrocartilage construct as well as the integration of construct-to-tendon (Fig. 4A). In contrast, detachment of scaffold-free fibrocartilage construct-to-tendon interface was observed in the group

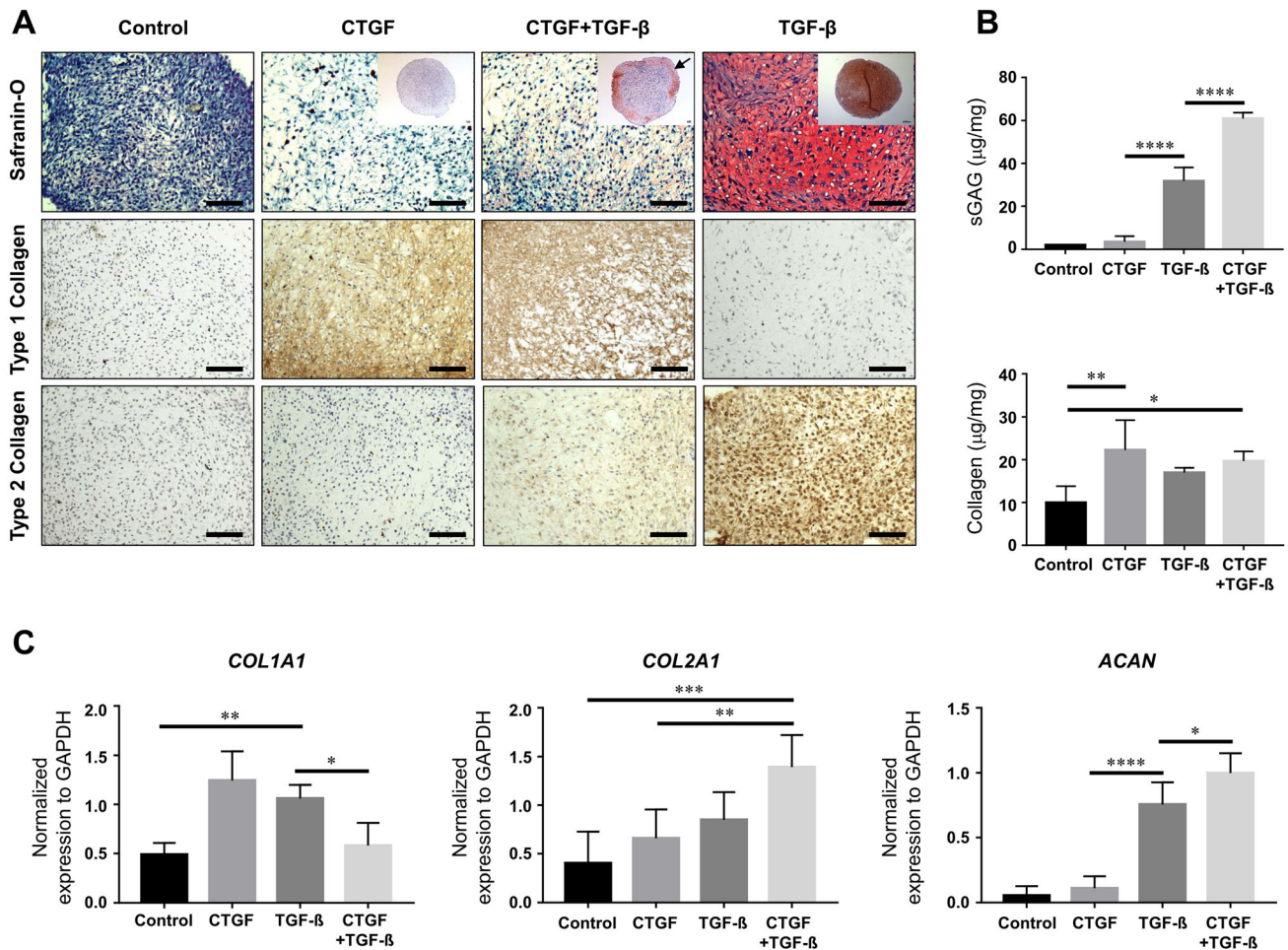


Fig. 2 *in vitro* characterization of fibrocartilage constructs according to two growth factors addition. **A** Histologic **B** biochemical characterization of fibrocartilage constructs. **C** Gene expressions were

quantified by qRT-PCR analysis. Differences among the groups were determined by one-way ANOVA with Turkey's multiple comparisons test (* $p < 0.05$, ** $p < 0.01$ and *** $p < 0.001$). Scale bar = 100 μ m

without collagenase treatment (Fig. 4A). The integration failure stress was significantly highest in the Col+D+ group, but there was no significant difference between other groups except empty group (Fig. 4B, Col+D+: 22.494 ± 13.74 Kpa, Empty: 0.46 ± 0.13 Kpa, Col-D-: 5.72 ± 1.76 Kpa, Col+D-: 7.41 ± 2.67 Kpa, and Col-D+: 7.93 ± 2.91 Kpa). Consequently, fibrocartilage differentiation and collagenase treatment mimicked native bone-to-tendon interface and promoted bone-to-scaffold-free fibrocartilage construct-to-tendon interface integration.

3.4 Bone-to-tendon healing efficacy *in vivo*

At week 2, ACL Recon group showed fibrous scar at BTI. In contrast, the representative hematoxylin and eosin (H&E) stained image of ACL Recon+FC group indicated hypercellular tissue mass attached directly bone and tendon (Fig. 5A). After 4 weeks, both groups showed enhanced integration between bone and tendon graft compared to 2

weeks. Particularly, the formation of hypercellular, fibrocartilage-like tissue was observed at the ACL Recon+ FC group (red arrow). In addition, safranin-O stained images showed increased sGAG deposition in the ACL Recon+FC group with the group compared to ACL Recon group (red arrowhead). The results of biomechanical test indicated the enhanced mechanical properties of both groups at 4 weeks operation compared to 2 weeks in line with histologic results (Fig. 5B). All knees failed at the BTI of the femoral tunnel during the biomechanical examination. In particular, the estimated stiffness of ACL Recon+FC group was increased by 88% ($p = 0.0102$) when compared to the ACL Recon group at 4 weeks operation. In all, histologic and biomechanical results showed improved integration in interface as well as fibrocartilaginous tissue formation at the group of ACL Recon+FC group.

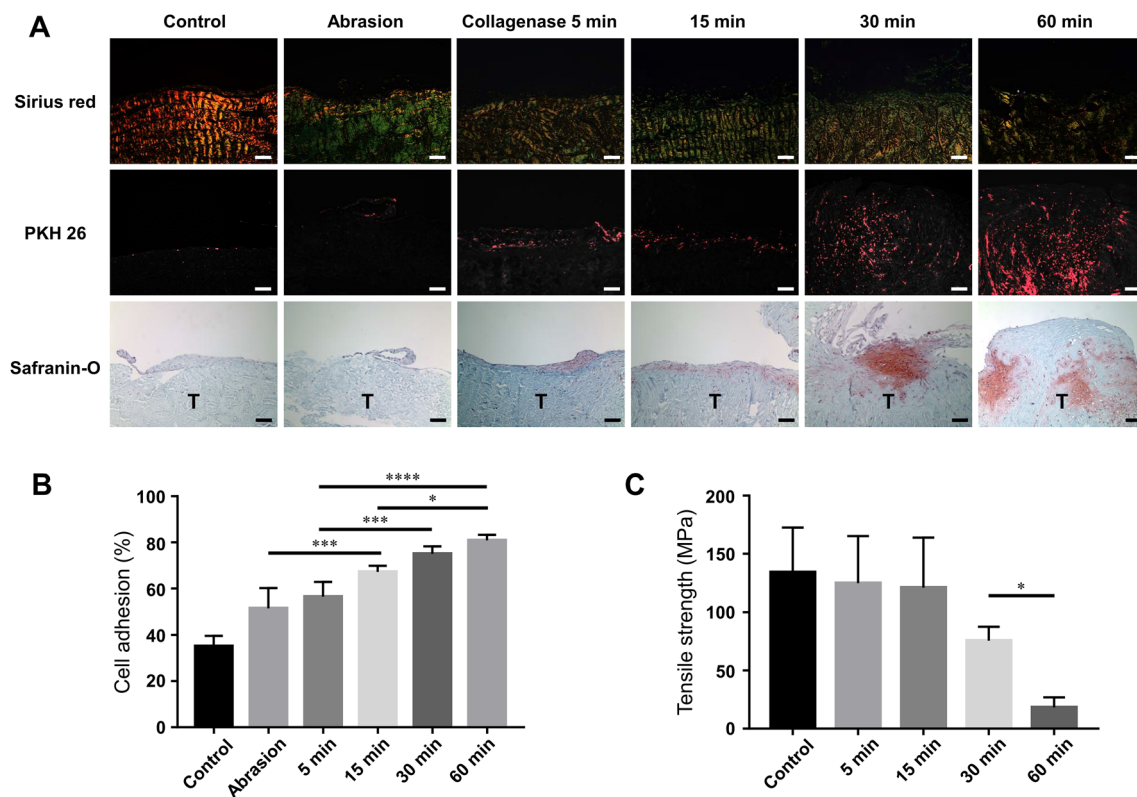


Fig. 3 Optimization of collagenase treatment time for enhanced integration of rSy-MSC to tendon. **A** Histological analysis of integration with rSy-MSCs and tendon and **B** quantitative analysis of PKH-labeled rSy-MSCs attachment to tendon and **C** biomechanical

evaluation of tendon after treatment of collagenase. Differences among the groups were determined by one-way ANOVA with Turkey's multiple comparisons test (* $p < 0.05$, ** $p < 0.01$ and *** $p < 0.001$). Scale bar = 100 μm

4 Discussion

The goal of this study was to engineer sy-MSC based scaffold-free fibrocartilage constructs and investigate its efficacy in an *in vivo* rat ACL reconstruction model. Treatment of both CTGF and TGF- β resulted in fibrocartilage differentiation of the scaffold-free constructs. Collagenase treatment on the tendon surface resulted in enhanced cell-to-tendon graft integration. Fibrocartilage constructs, together with tendon collagenase treatment resulted in BTI healing similar to native BTI and increased biomechanical strength compared to the current tendon reconstruction group both *in vitro* and *in vivo*. In all, scaffold-free fibrocartilage engineering together with tendon collagenase treatment offers a potential biomimetic solution to improve current tendon/ligament reconstructions.

Fibrocartilage, by definition, is a composite connective tissue with both fibrous and chondrogenic properties. A number of growth factor combinations utilizing BMP-2 [36], BMP-7 [37, 38], IGF-1 [39, 40], CTGF [41], and TGF- β 3 [42] have been used to induce fibrochondrogenic differentiation *in vitro* and *in vivo*. Lee et al. [43] described a sequential treatment protocol of CTGF followed by TGF-

β 3 treatment on MSCs to induce fibrochondrogenic differentiation in a scaffold-based model for meniscus regeneration. We have utilized a combination of CTGF and TGF- β condition media for fibrochondrogenic differentiation and have found both fibrous and cartilaginous properties within 2 weeks of *in vitro* culture in the respective scaffold-free constructs (Fig. 2). CTGF directs fibroblast differentiation in MSCs [44] while TGF- β 1 induces MSC condensation and chondrocyte differentiation. Fibrochondrogenic differentiation protocols may be influenced by MSC type, growth factor combinations and dosage, duration of differentiation, and culture conditions.

A sheath known as the paratenon covers most tendons which allow smooth gliding of the tendon via proteoglycan rich matrix [45]. These sheaths may deter BTI integration and are usually dissected off during ACL autograft reconstructions [35]. Previous studies have reported the effects of enzyme treatment on connective tissue surfaces such as collagenase [46, 47] and hyaluronidase [48] to improve integration. We observed that collagenase treatment time correlated with cell adhesion while inversely correlating to biomechanical strength of the graft. Collagenase treatment resulted in cells and surrounding tissue to interdigitate with the graft tissue, resembling native BTI

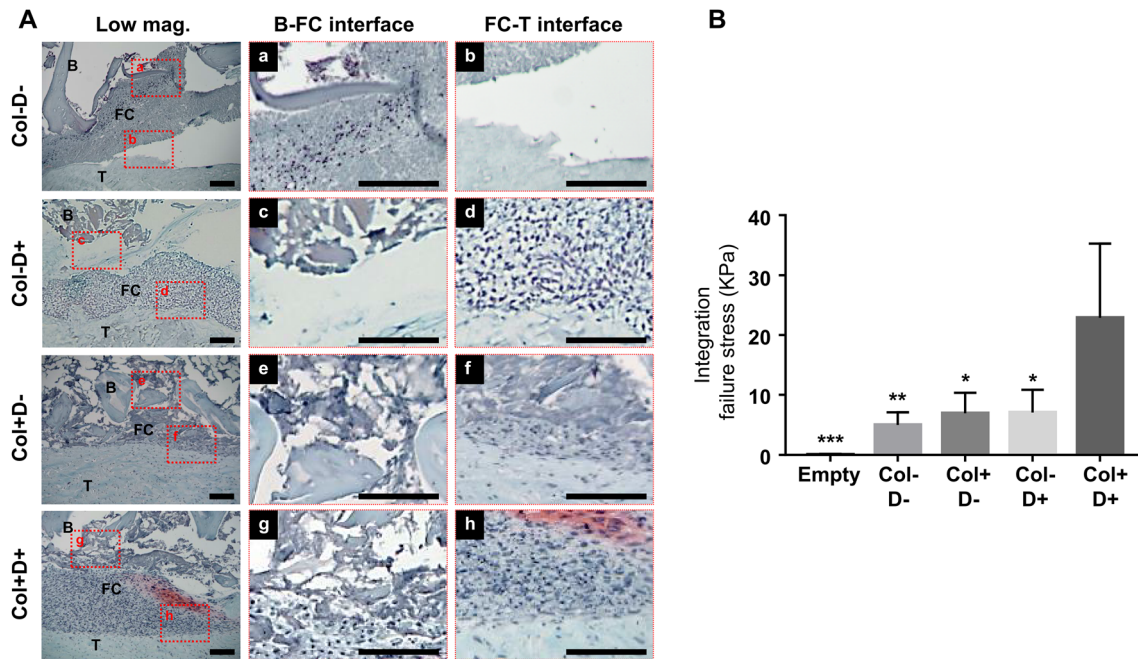


Fig. 4 Integration analysis of scaffold-free fibrocartilage construct *in vitro*. **A** The representative histologic images stained using safranin-O at integrated region as low magnification image (left) and high magnification images (right, a–h) **B** Quantification of failure stress after 4 weeks differentiation. Differences among the groups

were determined by one-way ANOVA with Turkey's multiple comparisons test ($*p < 0.05$, $**p < 0.01$ and $***p < 0.001$ compared to the Col + D + group). **B**; Bone, **T**; Tendon, **FC**; Fibrocartilage construct. Scale bar = 100 μ m

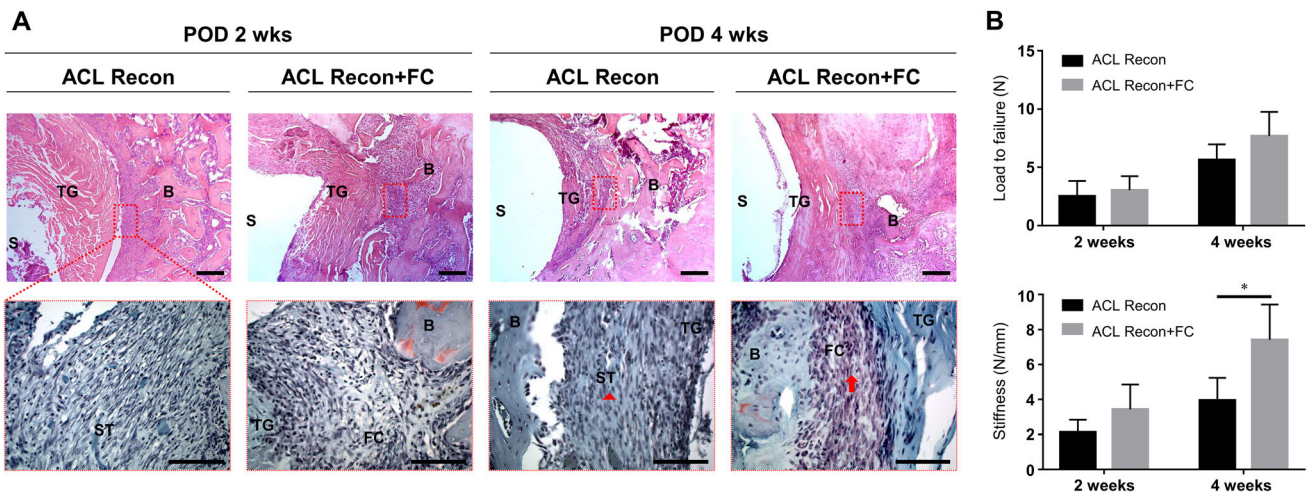


Fig. 5 Bone tendon healing efficacy *in vivo*. **A** The representative histological images stained with H&E and safranin-O at bone and tendon integrated region. The black rectangle indicates the region of interest for safranin-O stained images. Red arrow indicated fibrocartilage-like tissue at the ACL Recon + FC group, whereas arrowhead indicated increased sGAG deposition in the ACL Recon + FC group

with the group compared to ACL Recon group **B** the biomechanical evaluation for measuring load to failure and stiffness by using universal testing machine. **ST**; Scar tissue, **B**; Bone, **TG**; Tendon graft, **FC**; Fibrocartilage cell construct, and **S**; Screw. Scale bar = 100 μ m

(Fig. 3). Collagenase treatment, however, should be optimized to the graft being used and clinical scenarios to maximize the integration effect while minimizing biomechanical strength loss of the graft.

Regarding the rat ACL reconstruction model, we have utilized an interference screw to fix the graft to the bone

tunnel, following methods from previously reported studies [49, 50]. Interference screws are commonly used in human reconstructions to provide firm fixation and compression of the graft to the bone tunnel. We have utilized interference screws in our rat model to reduce motion of the graft within the bone tunnel, considering the soft cancellous bone of

rodents compared to humans. Furthermore, interference screws increased the reproducibility of the *in vivo* results by preventing migration and potential loss of the implanted construct. Histology and biomechanical analyses of both experiment groups were equally carried out after removal of the interference screws.

The mode of action of our constructs can be explained by biomimicry, which was achieved by fibrocartilaginous scaffold-free constructs and collagenase treatment of the tendon grafts. Fibrocartilage constructs mimicked the native fibrocartilage layers situated between the tendon and bone, while collagenase treatment resulted in interdigitating integration between the tendon graft and fibrocartilage constructs. The effect of these two factors was shown in the *in vitro* BTI model, where fibrocartilage constructs together with collagenase treatment resulted in the highest biomechanical strength in the BTI (Figs. 4B, 5B). Previous strategies attempted to improve BTI healing through enhanced osteogenesis, *in situ* tissue formation via scaffolds, or increased MSCs in the BTI. Several studies utilized growth factor delivery via biomaterials such as bone morphogenetic protein (BMP) [27, 38] and fibroblast growth factor (FGF) [51, 52], or insertion of nano-scaffolds [53, 54]. Some studies also tested the efficacy of sy-MSCs in BTI healing. Ouyang et al. observed higher percentage of oblique fiber formation after sy-MSC treatment in BTI but could not detect fibrocartilage formation until the week 4 of transplantation [25]. Wrapping the tendon graft with tendon-derived stem cell sheets also enhanced mineralized tissue formation inside bone tunnel thus facilitating early graft healing in a previous study [32]. Our study adds on such previous strategies in that we have attempted to engineer the BTI rather than deliver certain cells or growth factors. The use of scaffold-free constructs in turn may have a beneficial role in BTI engineering in terms of non-uniform application and prevention of cell loss [24].

This study has the following limitations. The rat ACL model used in this study does not reflect the human knee environment after major ligament reconstructions of the knee. Furthermore, longer observation time periods may be necessary to fully validate the fate of the implanted scaffold-free construct in the BTI. Guo et al. reported that the scaffold-free construct preserved cells from acute inflammation and ECM of the construct facilitated integration of host cells and neo-epicardial tissue [55]. While some researcher revealed the presence of MSC up to week 8 at the graft-to-bone tunnel interface in rat model [30], other reported the disappearance of transplanted MSC within 4 weeks [25]. Therefore, further research is required to identify the fate of cells after implantation by using cell tracking. Furthermore, the *in vivo* data could be improved with further biological and microstructural characterizations of the implanted construct. Collagen microstructure

and fiber orientation, as well as mineral density of the bone tunnel are important factors in BTI healing. Further investigations concerning such factors are required in a large animal model to further investigate the biomimicry potential of the constructs and potential areas for improvement.

Taken together, the implantation of scaffold-free fibrocartilage constructs at the BTI achieved considerable biomimicry, via fibrocartilage formation and collagenase treatment of the tendon graft. Future research directed to mimic the native BTI may further enhance clinical results of current tendon/ligament reconstruction.

Supplementary Information The online version contains supplementary material available at <https://doi.org/10.1007/s13770-023-00593-2>.

Acknowledgements This research was supported by National Research Foundation (NRF) funded by the Korean Government (MSIT) [2023R1A2C1007200 (D.Y.P.)] and Korea Health Technology R&D Project through the Korea Health Industry Development Institute (KHIDI), funded by the Ministry of Health and Welfare, Republic of Korea [HR22C1734]. This study was supported, in part, by a grant from the State of North Carolina.

Author's contributions The experiments were conceptualized and designed by SJL, DYP, and JJY; SN and DYP made significant contribution to the experiments. YJJ, and H-WY assisted with the experiments and data organization. The data analysis was carried out by SJL and DYP; SJL, B-HM, and J-YP contributed to the analysis through productive discussion. SN and DYP wrote the draft manuscript and revised the manuscript. All authors read and approved the final manuscript.

Data availability statement The data presented in this study are available on request from all the authors.

Declarations

Conflict of interest The authors declare that they have no conflicts of interest.

Ethical statement All animal procedures were performed according to the protocol (A16-141) approved by the Institutional Animal Care and Use Committee (IACUC) at Wake Forest University Health Sciences.

References

- Maffulli N, Wong J, Almekinders LC. Types and epidemiology of tendinopathy. *Clin Sports Med.* 2003;22:675–92.
- van der List JP, Mintz DN, DiFelice GS. The location of anterior cruciate ligament tears: a prevalence study using magnetic resonance imaging. *Orthop J Sports Med.* 2017;5:2325967117709966.
- Parkkari J, Pasanen K, Mattila VM, Kannus P, Rimpelä A. The risk for a cruciate ligament injury of the knee in adolescents and young adults: a population-based cohort study of 46 500 people with a 9 year follow-up. *Br J Sports Med.* 2008;42:422–6.
- Moses B, Orchard J, Orchard J. Systematic review: Annual incidence of ACL injury and surgery in various populations. *Res Sports Med.* 2012;20:157–79.

5. Chung KS, Kim JH, Kong DH, Park I, Kim JG, Ha JK. An increasing trend in the number of anterior cruciate ligament reconstruction in Korea: a nationwide epidemiologic study. *Clin Orthop Surg.* 2022;14:220–6.
6. Rayan F, Nanjayan SK, Quah C, Ramoutar D, Konan S, Haddad FS. Review of evolution of tunnel position in anterior cruciate ligament reconstruction. *World J Orthop.* 2015;6:252–62.
7. Kim JG, Kang SH, Kim JH, Lim CO, Wang JH. Comparison of clinical results, second-look arthroscopic findings, and MRI findings between the transportal and outside-in techniques for double-bundle anatomic anterior cruciate ligament reconstruction: a prospective, randomized controlled trial with a minimum 2-year follow-up. *Am J Sports Med.* 2018;46:544–56.
8. Liukkonen RJ, Ponkilainen VT, Reito A. Revision rates after primary ACL reconstruction performed between 1969 and 2018: a systematic review and metaregression analysis. *Orthop J Sports Med.* 2022;10:23259671221110190.
9. Di Benedetto P, Di Benedetto E, Fiocchi A, Beltrame A, Causero A. Causes of failure of anterior cruciate ligament reconstruction and revision surgical strategies. *Knee Surg Relat Res.* 2016;28:319–24.
10. Yin Z, Chen X, Zhu T, Hu JJ, Song HX, Shen WL, et al. The effect of decellularized matrices on human tendon stem/progenitor cell differentiation and tendon repair. *Acta Biomaterialia.* 2013;9:9317–29.
11. Castricini R, Longo UG, De Benedetto M, Panfoli N, Pirani P, Zini R, et al. Platelet-rich plasma augmentation for arthroscopic rotator cuff repair: a randomized controlled trial. *Am J Sports Med.* 2011;39:258–65.
12. Font Tellado S, Balmayor ER, Van Griensven M. Strategies to engineer tendon/ligament-to-bone interface: Biomaterials, cells and growth factors. *Adv Drug Deliv Rev.* 2015;94:126–40.
13. Jiang X, Kong Y, Kuss M, Weisenburger J, Haider H, Harms R, et al. 3D bioprinting of multilayered scaffolds with spatially differentiated ADMSCs for rotator cuff tendon-to-bone interface regeneration. *Appl Mater Today.* 2022;27:101510.
14. Du L, Qin C, Zhang H, Han F, Xue J, Wang Y, et al. Multicellular bioprinting of biomimetic inks for tendon-to-bone regeneration. *Adv Sci.* 2023;10:2301309.
15. Balestri W, Hickman GJ, Morris RH, Hunt JA, Reinwald Y. Triphasic 3D in vitro model of bone-tendon-muscle interfaces to study their regeneration. *Cells.* 2023;12:313.
16. Xu X, Si Y, Zhao Y, Ke Q, Hu J. Electrospun textile strategies in tendon to bone junction reconstruction. *Adv Fiber Mater.* 2023;5:764–90.
17. Yang R, Zheng Y, Zhang Y, Li G, Xu Y, Zhang Y, et al. Bipolar metal flexible electrospun fibrous membrane based on metal-organic framework for gradient healing of tendon-to-bone interface regeneration. *Adv Healthcare Mater.* 2022;11:2200072.
18. Soo Kim B, Ji Kim E, Suk Choi J, Hoon Jeong J, Hyunchul Jo C, Woo CY. Human collagen-based multilayer scaffolds for tendon-to-bone interface tissue engineering. *J Biomed Mater Res, Part A.* 2014;102:4044–54.
19. Li X, Xie J, Lipner J, Yuan X, Thomopoulos S, Xia Y. Nanofiber scaffolds with gradations in mineral content for mimicking the tendon-to-bone insertion site. *Nano Lett.* 2009;9:2763–8.
20. Zhang H, Ma Y, Wang Y, Niu L, Zou R, Zhang M, et al. Rational design of soft-hard interfaces through bioinspired engineering. *Small.* 2023;19:2204498.
21. Han F, Zhang P, Sun Y, Lin C, Zhao P, Chen J. Hydroxyapatite-doped polycaprolactone nanofiber membrane improves tendon-to-bone interface healing for anterior cruciate ligament reconstruction. *Int J Nanomedicine.* 2015;10:7333–43.
22. Chung EJ, Sugimoto MJ, Koh JL, Ameer GA. A biodegradable tri-component graft for anterior cruciate ligament reconstruction. *J Tissue Eng Regen Med.* 2017;11:704–12.
23. Erickson IE, Kestle SR, Zellars KH, Dodge GR, Burdick JA, Mauck RL. Improved cartilage repair via in vitro pre-maturation of MSC-seeded hyaluronic acid hydrogels. *Biomed Mater.* 2012;7: 024110.
24. Mifune Y, Matsumoto T, Takayama K, Terada S, Sekiya N, Kuroda R, et al. Tendon graft revitalization using adult anterior cruciate ligament (ACL)-derived CD34+ cell sheets for ACL reconstruction. *Biomaterials.* 2013;34:5476–87.
25. Ju YJ, Muneta T, Yoshimura H, Koga H, Sekiya I. Synovial mesenchymal stem cells accelerate early remodeling of tendon-bone healing. *Cell Tissue Res.* 2008;332:469–78.
26. Ouyang HW, Goh JC, Lee EH. Use of bone marrow stromal cells for tendon graft-to-bone healing: histological and immunohistochemical studies in a rabbit model. *Am J Sports Med.* 2004;32:321–7.
27. Chen CH, Liu HW, Tsai CL, Yu CM, Lin IH, Hsiue GH. Photoencapsulation of bone morphogenetic protein-2 and periosteal progenitor cells improve tendon graft healing in a bone tunnel. *Am J Sports Med.* 2008;36:461–73.
28. Li F, Jia H, Yu C. ACL reconstruction in a rabbit model using irradiated Achilles allograft seeded with mesenchymal stem cells or PDGF-B gene-transfected mesenchymal stem cells. *Knee Surg Sports Traumatol Arthrosc.* 2007;15:1219–27.
29. Mifune Y, Matsumoto T, Ota S, Nishimori M, Usas A, Kopf S, et al. Therapeutic potential of anterior cruciate ligament-derived stem cells for anterior cruciate ligament reconstruction. *Cell Transplant.* 2012;21:1651–65.
30. Li YG, Wei JN, Lu J, Wu XT, Teng GJ. Labeling and tracing of bone marrow mesenchymal stem cells for tendon-to-bone tunnel healing. *Knee Surg Sports Traumatol Arthrosc.* 2011;19:2153–8.
31. Soon MY, Hassan A, Hui JH, Goh JC, Lee EH. An analysis of soft tissue allograft anterior cruciate ligament reconstruction in a rabbit model: a short-term study of the use of mesenchymal stem cells to enhance tendon osteointegration. *Am J Sports Med.* 2007;35:962–71.
32. Lui PP, Wong OT, Lee YW. Application of tendon-derived stem cell sheet for the promotion of graft healing in anterior cruciate ligament reconstruction. *Am J Sports Med.* 2014;42:681–9.
33. Shaw HM, Benjamin M. Structure-function relationships of entheses in relation to mechanical load and exercise. *Scand J Med Sci Sports.* 2007;17:303–15.
34. Park DY, Min BH, Park SR, Oh HJ, Truong MD, Kim M, et al. Engineered cartilage utilizing fetal cartilage-derived progenitor cells for cartilage repair. *Sci Rep.* 2020;10:5722.
35. Chahla J, Moatshe G, Cinque ME, Godin J, Mannava S, LaPrade RF. Arthroscopic anatomic single-bundle anterior cruciate ligament reconstruction using bone-patellar tendon-bone autograft: pearls for an accurate reconstruction. *Arthrosc Tech.* 2017;6:e1159–67.
36. Minehara H, Urabe K, Naruse K, Mehlhorn AT, Uchida K, Südkamp NP, et al. A new technique for seeding chondrocytes onto solvent-preserved human meniscus using the chemokinetic effect of recombinant human bone morphogenetic protein-2. *Cell Tissue Bank.* 2011;12:199–207.
37. Forriol F, Ripalda P, Duarte J, Esparza R, Gortazar AR. Meniscal repair possibilities using bone morphogenetic protein-7. *Injury.* 2014;45:S15–21.
38. Ozeki N, Muneta T, Koga H, Katagiri H, Otobe K, Okuno M, et al. Transplantation of achilles tendon treated with bone morphogenetic protein 7 promotes meniscus regeneration in a rat model of massive meniscal defect. *Arthritis Rheum.* 2013;65:2876–86.
39. Puetzer JL, Brown BN, Ballyns JJ, Bonassar LJ. The effect of IGF-I on anatomically shaped tissue-engineered menisci. *Tissue Eng Part A.* 2013;19:1443–50.

40. Zhang H, Leng P, Zhang J. Enhanced meniscal repair by over-expression of hGF-1 in a full-thickness model. *Clin Orthop Relat Res.* 2009;467:3165–74.
41. He W, Liu YJ, Wang ZG, Guo ZK, Wang MX, Wang N. Enhancement of meniscal repair in the avascular zone using connective tissue growth factor in a rabbit model. *Chin Med J (Engl).* 2011;124:3968–75.
42. Ionescu LC, Lee GC, Huang KL, Mauck RL. Growth factor supplementation improves native and engineered meniscus repair in vitro. *Acta Biomater.* 2012;8:3687–94.
43. Lee CH, Rodeo SA, Fortier LA, Lu C, Erisken C, Mao JJ. Protein-releasing polymeric scaffolds induce fibrochondrocytic differentiation of endogenous cells for knee meniscus regeneration in sheep. *Sci Transl Med.* 2014;6:266ra171.
44. Lee CH, Shah B, Moioli EK, Mao JJ. CTGF directs fibroblast differentiation from human mesenchymal stem/stromal cells and defines connective tissue healing in a rodent injury model. *J Clin Invest.* 2010;120:3340–9.
45. Puxkandl R, Zizak I, Paris O, Keckes J, Tesch W, Bernstorff S, et al. Viscoelastic properties of collagen: synchrotron radiation investigations and structural model. *Philos Trans R Soc Lond B Biol Sci.* 2002;357:191–7.
46. Janssen LM, In der Maur CD, Bos PK, Hardillo JA, van Osch GJ. Short-duration enzymatic treatment promotes integration of a cartilage graft in a defect. *Ann Otol Rhinol Laryngol.* 2006;115:461–8.
47. van de Breevaart Bravenboer J, In der Maur CD, Bos PK, Feenstra L, Verhaar JA, Weinans H, et al. Improved cartilage integration and interfacial strength after enzymatic treatment in a cartilage transplantation model. *Arthritis Res Ther.* 2004;6:R469–76.
48. Bos PK, DeGroot J, Budde M, Verhaar JA, van Osch GJ. Specific enzymatic treatment of bovine and human articular cartilage: implications for integrative cartilage repair. *Arthritis Rheum.* 2002;46:976–85.
49. Flury A, Wild L, Waltenspül M, Zindel C, Vlachopoulos L, Imhoff FB, et al. Tibial tunnel enlargement is affected by the tunnel diameter-screw ratio in tibial hybrid fixation for hamstring ACL reconstruction. *Arch Orthop Trauma Surg.* 2023;143:1923–30.
50. Herrera A, Martínez F, Iglesias D, Cegoñino J, Ibarz E, Gracia L. Fixation strength of biocomposite wedge interference screw in ACL reconstruction: effect of screw length and tunnel/screw ratio. A controlled laboratory study. *BMC Musculoskeletal Disorders.* 2010;11:139.
51. Atesok K, Fu FH, Wolf MR, Ochi M, Jazrawi LM, Doral MN, et al. Augmentation of tendon-to-bone healing. *J Bone Joint Surg Am.* 2014;96:513–21.
52. Kamalidinov TB, Fujino K, Shetye SS, Jiang X, Ye Y, Rodriguez AB, et al. Amplifying bone marrow progenitors expressing α -smooth muscle actin produce zonal insertion sites during tendon-to-bone repair. *J Orthop Res.* 2020;38:105–16.
53. Zhu Q, Ma Z, Li H, Wang H, He Y. Enhancement of rotator cuff tendon-bone healing using combined aligned electrospun fibrous membranes and kartogenin. *RSC Adv.* 2019;9:15582–92.
54. Zhao S, Xie X, Pan G, Shen P, Zhao J, Cui W. Healing improvement after rotator cuff repair using gelatin-grafted poly(L-lactide) electrospun fibrous membranes. *J Surg Res.* 2015;193:33–42.
55. Guo R, Wan F, Morimatsu M, Xu Q, Feng T, Yang H, et al. Cell sheet formation enhances the therapeutic effects of human umbilical cord mesenchymal stem cells on myocardial infarction as a bioactive material. *Bioactive Materials.* 2021;6:2999–3012.

Publisher's Note Springer Nature remains neutral with regard to jurisdictional claims in published maps and institutional affiliations.

Springer Nature or its licensor (e.g. a society or other partner) holds exclusive rights to this article under a publishing agreement with the author(s) or other rightsholder(s); author self-archiving of the accepted manuscript version of this article is solely governed by the terms of such publishing agreement and applicable law.